Anisotropic magnetotransport in $SrTiO_3$ surface electron gases generated by Ar^+ irradiation

F. Y. Bruno,[1] J. Tornos,[1] M. Gutierrez del Olmo,[1] G. Sanchez Santolino,[1] N. M. Nemes,[1] M. Garcia-Hernandez,[2] B. Mendez,[3] J. Piqueras,[3] G. Antorrena,[4] L. Morellón,[4,5] J. M. De Teresa,[5,6] M. Clement,[7] E. Iborra,[7] C. Leon,[1] and J. Santamaria[1]

[1]*GFMC, Departamento Fisica Aplicada III, Universidad Complutense de Madrid, E-28040 Madrid, Spain*

[2]*Instituto de Ciencia de Materiales de Madrid, Consejo Superior de Investigaciones Cientificas, E-28049 Cantoblanco, Spain*

[3]*Departamento Fisica de Materiales, Universidad Complutense de Madrid, E-28040 Madrid, Spain*

[4]*Instituto de Nanociencia de Aragón (INA), Universidad de Zaragoza, Zaragoza E-50018, Spain*

[5]*Instituto de Ciencia de Materiales de Aragón (ICMA), Universidad de Zaragoza–CSIC, Zaragoza E-50009, Spain*

[6]*Departamento de Física de la Materia Condensada, Universidad de Zaragoza, Zaragoza E-50009, Spain*

[7]*ETSIT Universidad Politecnica de Madrid, E-28040 Madrid, Spain*

(Received 2 December 2010; revised manuscript received 4 March 2011; published 23 June 2011)

Metallic surface layers are fabricated by doping (100) $SrTiO_3$ (STO) single crystals with oxygen vacancies generated by bombardment with Ar ions from an rf plasma source. The presence of oxygen vacancies is confirmed by cathodoluminescence and x-ray photoemission spectroscopy. This technique produces a surface electron gas with high values of the sheet carrier density ($n_{2D} = 2.45\times10^{17}$ cm^{-2}). A strong increase (300%) of the low-temperature magnetoresistance is observed when the magnetic field is rotated away from the surface, characteristic of orbital effects of confined electrons. We estimate the width of the confinement region to be in the 200–300 nm range. When a magnetic field is applied in the surface plane and parallel to the current direction, a large negative magnetoresistance is found below the structural transition of the STO, which is discussed in terms of spin-orbit scattering. On further reduction of temperature, there is a change to a positive magnetoresistance regime due to the scattering of charge carriers at the disordered surface region.

DOI: 10.1103/PhysRevB.83.245120 PACS number(s): 71.10.Ca, 68.47.Gh

I. INTRODUCTION

The difficulties of semiconductor electronics in maintaining the pace of increase of the integration density and computer processing speed have triggered an important effort in the search for alternative materials and device concepts. Oxide electronics is an emerging field embracing strategies to overcome the limitations of silicon devices using correlated transition metal oxides. Complex oxides constitute an interesting family of materials, whose rich phase diagrams allow the design of devices with novel functionalities. Among the different oxides, $SrTiO_3$ (STO) is a very important (semiconductor) material, not only as a commonly used substrate but also as an active layer in new epitaxial architectures with interesting properties. Its semiconducting character and possibility of doping result from the mixed valence of the Ti.[1] Conducting electrons are supplied by anion substitution (typically Ti by Nb and Sr by La) or by oxygen removal. The possibility of growing this material epitaxially on Si[2] is an important step toward the compatibility of oxide electronics with current silicon complementary metal-oxide-semiconductor technology. The recent finding of a two-dimensional (2D) electron gas at the $LaAlO_3/SrTiO_3$ interface[3] with an electrostatically tunable carrier density[4,5] has increased the interest in this material even more. There is general agreement that it results from doping the STO at the interface, although the detailed mechanism (oxygen vacancies, intermixing, or charge transfer due to polar catastrophe) remains a subject of debate.[6–8]

As a distinct route for doping STO, Ar ion milling, has been recently shown to transform insulating single crystals into a transparent conductor, presumably as the result of oxygen vacancies generated by ion beam etching.[9] Excess electrons associated with oxygen removal can be trapped at Ti bonds upon a change in the oxidation state from +4 to +3 (neutral vacancy state) or transferred to the conduction band (positively charged vacancy state), making the material conducting. This procedure makes use of the small etch rate and short penetration of low-energy ions to create large doses over a narrow layer. The confined 2D transport proposed within such a thin layer is highly interesting because it provides a direct procedure to fabricate 2D electron gases in STO layouts. For energies above 200 eV the low-resistivity state is independent of the energy or irradiation time. This suggests a disordered surface layer, over which vacancies are generated within a thickness that does not increase as the etch process progresses. This thickness is determined by the ion penetration depth: a few nanometers in this energy range. Oxygen vacancies generated within the disordered layer supply carriers that become delocalized over much larger distances due to the screening of the space charge (neutrality restoring) potential by the large permittivity of the STO.[10] More recently, Ngai *et al.*[11] have reported the effect of gate voltage on the transport properties of STO single crystals doped by Ar^+ bombardment, showing that the electric field modulates the scattering potential through its effect on the dielectric permittivity of STO, enabling control of the mobility in a wide range.

In this paper we examine the anisotropic magnetotransport of conducting STO single crystals with a low-resistivity state generated by ion milling with Ar^+ ions supplied by a rf plasma source. This irradiation technique yields samples with sheet carrier densities several (2–3) orders of magnitude larger than in previous reports.[9] The high doping level allows us to explore additional transport regimes. A strong anisotropy of the angular dependence of the magnetoresistance (MR) characteristic of orbital effects of electrons confined in a thin layer is found when the magnetic field is rotated away from the surface plane. For in-plane magnetic fields aligned with the

direction of the injected current, an anomalous (large) negative magnetoresistance is found below the structural transition of the STO, which is explained in terms of spin-orbit scattering by localized Ti^{3+} moments in the confinement region. This term crosses over into a positive magnetoresistance contribution when temperature is further reduced, which is discussed in terms of scattering by the disordered region at the surface.

II. EXPERIMENT

Samples, commercial STO single crystals (001), were chemically etched and annealed following the standard recipe to ensure a TiO_2 surface termination.[12] Atomic force microscopy (AFM) imaging showed the presence of well-defined terraces. Samples were introduced into an Ar ion milling reactor and etched for periods of 5 min under an Ar pressure of 2 mTorr and at rf powers increasing from 20 to 60 W. Crystals, originally insulating, become conducting for powers above the 25 W level with little change in the 30–50 W range. After bombardment, the surface did not show the terrace structure any longer. Cathodoluminescence (CL) spectra were recorded with a Hamamatsu PMA-11 charge-coupling device camera in a Hitachi S-2500 scanning electron microscope (SEM). The operation conditions used were 5 keV for electron beam energy and 1–5 nA beam current. X-ray photoemission spectroscopy (XPS) analysis was conducted on a Kratos AXIS ultra DLD XPS spectrometer using monochrome Al $K\alpha$ radiation. High-resolution scans were performed using 100 meV energy steps at a 20 eV pass. The hybrid-slot mode employed supplies chemical information on a surface of $300 \times 700\ \mu m^2$. High-resolution spectra were acquired using a charge neutralizer, and as a result spectra had to be calibrated in energy. C 1*s* at 284.9 eV was used as a reference. The Ar-irradiated sample was compared with a pristine STO substrate and a Nb-doped STO crystal. Electrical transport was measured in the van der Pauw geometry using evaporated Al contacts. *IV* curves were recorded to ensure their Ohmic nature. Magnetoresistance was measured in a commercial apparatus (physical properties measurement system, Quantum Design) equipped with a rotating sample holder.

III. RESULTS AND DISCUSSION

Figure 1(a) shows the temperature dependence of the zero-field sheet resistance of a typical sample irradiated at a power of 30 W during 5 min, showing a metallic behavior in the whole temperature range. Four-probe measurements gave a low-temperature sheet resistance $R_{sq,5K} = 2.2\times10^{-2}\ \Omega$/sq. A power law T^2 dependence of the resistance characteristic of electron-electron scattering[13] is found below the STO structural transition as well as a large residual resistivity ratio $[\rho(300\ K)/\rho(5\ K) = 300]$. These low sheet resistance values are characteristic of doped samples and in fact, as also found by Reagor and Butko,[9] samples acquired a black color upon irradiation. Samples become transparent after annealing at 900 °C in oxygen, thus confirming that the conducting state is due to oxygen vacancies. Hall effect and magnetoresistance were measured in a magnetic field applied perpendicular to the crystal surface. Data were symmetrized and antisymmetrized for the magnetoresistance and Hall effect, respectively, to correct for spurious signals due to contacts or field misalignments. Figures 1(b) and 1(c) show typical sets of measurements for the same sample at different temperatures. Combined magnetoresistance and Hall measurements were used to obtain mobility and sheet carrier density, with values $\mu_{5K} = 1699\ cm^2/V\ s$ and $n_{2D,5K} = 2.45\times10^{17}\ cm^{-2}$. We stress that our values of the sheet resistance are several orders of magnitude smaller than those found previously using Ar ion beam preferential etching instead of rf plasma ion milling,[9,11] suggesting that here oxygen vacancies are generated over a much wider length scale. Also, similar low values of the sheet resistance were found in $LaAlO_3$ (LAO)/STO interfaces grown in low oxygen pressures and have been discussed in terms of oxygen vacancies.[14] Conducting-tip AFM of LAO/STO showed that the conducting region extends about 1 μm into the bulk of the substrate,[14] indicating that the low-pressure growth generates substantial amounts of oxygen vacancies that diffuse from the surface to the interior of the crystal.

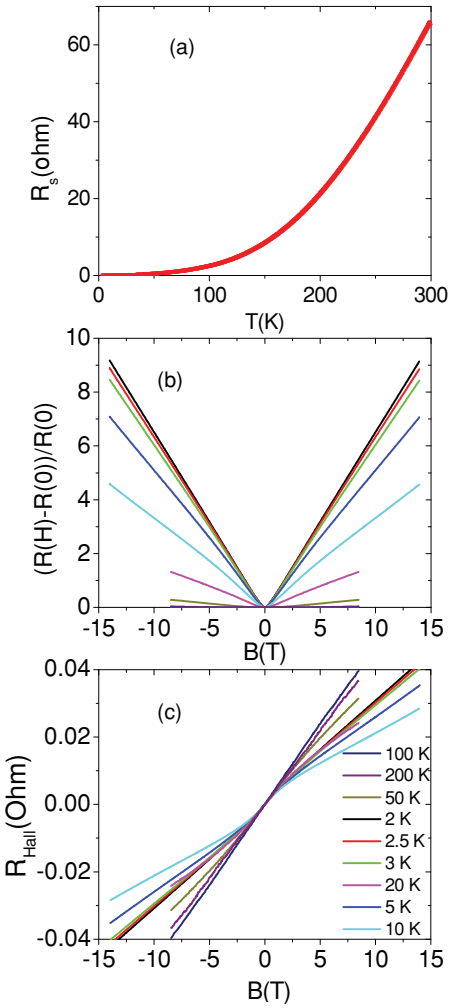

FIG. 1. (Color online) (a) Temperature dependence of the sheet resistance in zero applied magnetic field of STO crystals irradiated at a power of 30 W for 5 min. Magnetic field dependence of the 4 probe (van der Pauw) magnetoresistance at 200, 100, 50, 20, 10, 5, 3, 2.5 and 2 K (from bottom to top) (b) and Hall effect at 100, 200, 50, 2, 2.5, 3, 20, 5, and 10 (from bottom to top at 8 T) (c) in magnetic fields applied perpendicular to the crystal surface.

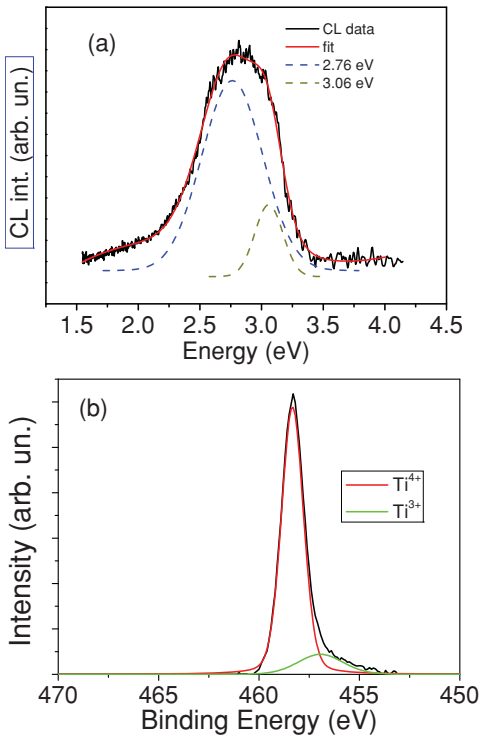

FIG. 2. (Color online) (a) Cathodoluminescence spectrum of Ar^+-irradiated STO sample at 220 K recorded with an acceleration voltage of 5 keV. Fit (continuous line) using Gaussian components (dotted lines) with maximum peaks at 2.76 and 3.06 eV. (b) High-resolution XPS Ti $2p_{3/2}$ spectra. Peaks were fitted to Gaussian-Lorentzian combinations. The peak centered at about 458.3 eV corresponds to Ti^{4+}, and the peak centered at a binding energy 1.4 eV below the Ti^{4+} peak was ascribed to Ti^{3+}.

CL measurements of STO samples were performed in the scanning electron microscope with 5 and 10 keV electron beam energy. Figure 2(a) shows the CL spectrum for an Ar^+-irradiated STO sample recorded at 5 keV, while no CL signal was detected for 10 keV. The emission consists of a composed band in the blue region, which could be deconvoluted into two components with peaks at 2.76 and 3.06 eV. The higher-energy component is close to the band gap intrinsic luminescence in STO and it is a weak shoulder of the main emission band peaked at 2.76 eV. This blue emission is related to radiative transitions involving oxygen vacancy levels created as a consequence of Ar irradiation. Green and blue luminescence bands have been reported in doped STO and were mainly attributed to oxygen vacancy centers.[15,16] However, there is still controversy about the underlying luminescence processes responsible for each emission band.[17] The accelerating voltage used to excite the CL signal is directly related to the electron penetration depth below the surface. We have carried out simulations of the penetration depth profiles using the CASINO software package[18] for 5 and 10 keV electrons in STO. Electrons accelerated with energy of 5 and 10 keV in STO probed a region of up to 200 and 500 nm, respectively, in depth below the sample surface. Hence, these results indicate that radiative centers induced by Ar irradiation were within a shallow layer ~100 nm thick below the surface.

XPS measurements were conducted on irradiated samples to examine changes in the Ti oxidation associated with the presence of oxygen vacancies. This technique consists of analyzing photoelectrons emitted by a sample illuminated with x rays and supplies chemical information from a layer about 5 nm underneath the surface with a 5%–10% accuracy. High-resolution XPS Ti $2p$ spectra were acquired to obtain information about the Ti oxidation state. Peaks were fitted to Gaussian-Lorentzian combinations and Shirley functions were used to fit the background [see Fig. 2(b)]. Three samples were examined, an as-received STO single crystal, a Nb-doped (0.1 wt %) crystal, and an irradiated crystal. Spectra corresponding to pristine STO and Nb-doped crystals were consistently analyzed in terms of a single Ti^{4+} species. The strongest signal corresponding to $2p_{3/2}$ is centered at about 458.3 eV and the $2p_{1/2}$ at 464.1 eV. The 5.8 eV splitting is consistent with a major presence of Ti^{4+}. In the Ar-irradiated sample fits required including a peak centered at a binding energy 1.4 eV below the Ti^{4+} peaks, which was ascribed to Ti^{3+}. Relative spectral weights were consistent with an 87.5/12.5 Ti^{4+}/Ti^{3+} ratio, indicating a strong electron doping of the surface layer which suggests a large amount of oxygen vacancies (0.0625 per formula) in this layer. We want to stress that, although most oxygen vacancies are generated within this surface layer, substantial Ti doping may extend deep into the layer away from this disordered surface layer due to the screening by the large values of the dielectric permittivity.

We now examine the anisotropic magnetotransport under a large applied magnetic field of 8.5 T. Figure 3 shows the angular dependence of the magnetoresistance when the magnetic field is rotated by an angle ϕ around an in-plane axis perpendicular to the current direction. For $\phi = 90^\circ$ the magnetic field is perpendicular to the front surface of the crystal and when $\phi = 0^\circ$ it is parallel to the current direction. Resistance curves were normalized to the resistance value in zero field, to compare data at different temperatures. As displayed in Fig. 3, the MR displays a $\sin^2$-like angular dependence when the magnetic field rotates from the in-plane direction (zero Lorentz force) to the transverse direction (maximum Lorentz force) with a strongly temperature-dependent amplitude. The small negative values around $\phi = 0^\circ$ in Fig. 3(a) result from a negative magnetoresistance for magnetic fields parallel to current in the temperature range (approx.) 15–50 K. This effect is discussed later in this paper. While room temperature data appear quite flat in this graph, resistance increases in excess of 300% are observed at low temperatures. Figure 3(b) shows the amplitude of MR change, i.e., the relative resistance change when the field is rotated from $\phi = 90^\circ$ to $\phi = 0^\circ$ as a function of temperature. The largest resistance changes occur below 100 K, and appear to saturate at low temperatures. This seems to coincide with the (104 K) cubic-to-tetragonal structural transition of the STO occurring as the result of rigid rotation of TiO_6 octahedra around the c axis in opposite directions, which can be as large as 2° at low temperatures. Mobility has been reported to increase quite significantly below the structural transition.[19] The large positive magnetoresistance with magnetic field perpendicular to the plane is several orders of magnitude larger than the weak magnetoresistance (of the order of 0.01%) found in doped bulk STO crystals and resulting from the ellipsoidal constant-energy surfaces with

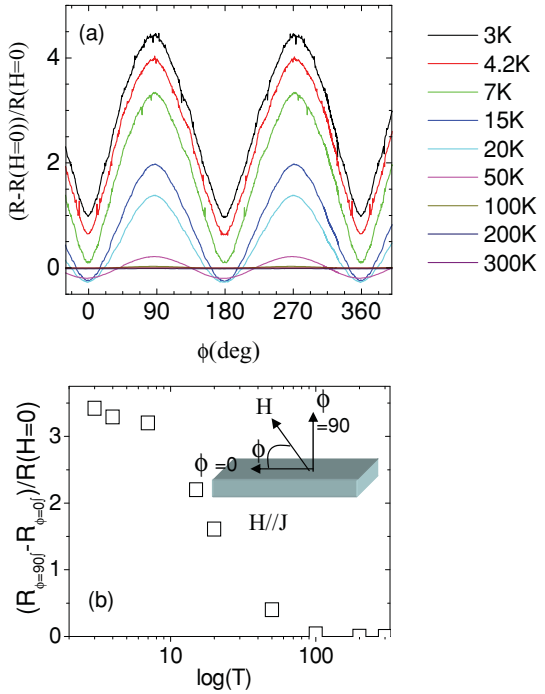

FIG. 3. (Color online) (a) Angular dependence of the magnetoresistance when the magnetic field of 8.5 T is rotated around an in-plane axis perpendicular to the current direction. As shown in the sketch for an angle $\phi = 90^\circ$ the magnetic field is perpendicular to the front surface of the crystal and for $\phi = 0^\circ$ it is parallel to the current direction. Different data sets are measurements at different temperatures (3, 4.2, 7, 15, 20, 50, 100, 200, 300 K from top to bottom at 90°) of a crystal irradiated at 30 W. Data are normalized to the zero-field resistance for comparison at different temperatures as $R_{\text{norm}}(\varphi) = [R(\varphi) - R(H = 0)]/R(H = 0)$. (b) Amplitude of angular magnetoresistance change according to $MR_\perp = [R(\varphi = 90^\circ) - R(\varphi = 0^\circ)]/R(H = 0)$ as a function of temperature.

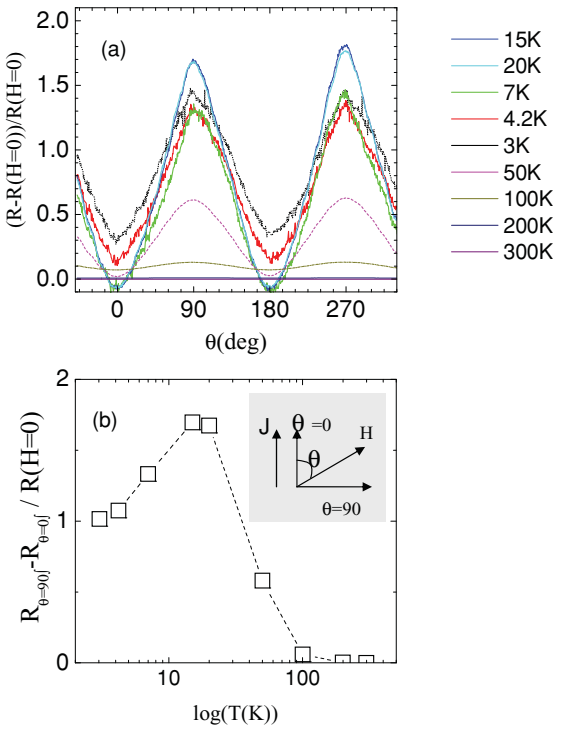

FIG. 4. (Color online) (a) Angular dependence of the magnetoresistance in an in-plane magnetic field of 8.5 T. As shown in the sketch, for an angle $\theta = 0$ the magnetic field is parallel to the current direction and for $\theta = 90^\circ$ it is perpendicular. Different data sets are measurements at different temperatures (15, 20, 7, 4.2, 3, 50, 100, 200, 300 K from top to bottom at 90°) of a crystal irradiated at 30 W. Data are normalized to the zero-field resistance $R_{\text{norm}}(\theta) = [R(\theta) - R(H = 0)]/R(H = 0)$. (b) Amplitude of the angular magnetoresistance change according to $MR = [R(\theta = 90^\circ) - R(\theta = 0^\circ)]/R(H = 0)$ as a function of temperature.

the long axes along [100] directions.[20,21] Rather, these very large magnetoresistance changes are characteristic of orbital effects of electrons in a confined geometry and most likely reflect that, as suggested earlier,[9] disorder generated by ion bombardment dopes the material over a narrow sheet at the crystal surface.

Further evidence of the low-dimensional nature of the electronic transport is obtained from magnetoresistance measurements with the magnetic field rotated within the surface plane. Figure 4(a) shows the angular dependence of the magnetoresistance when a magnetic field of 8.5 T is rotated in the plane of the crystal surface, at various temperatures. A nearly 100% increase of the magnetoresistance is found when the magnetic field reorients from parallel ($\theta = 0^\circ$) to perpendicular to the current ($\theta = 90^\circ$). As in the previous case of out-of-plane rotation of the magnetic field, there is a sharp increase of the magnetoresistance below the structural transition of the STO. Whereas there is no Lorentz force when H is parallel to the current density J, the Lorentz force is perpendicular to the surface when H is perpendicular to J, and orbital effects are expected for finite thickness of the confinement zone, t.[22] Thus, a parallel magnetic field in the surface plane does couple to the orbital degree of freedom of the system when the classical radius of the orbits is smaller that the width of the confinement region. At low temperatures, a clear decrease of the amplitude of resistance change can be readily observed when the magnetic field is rotated in plane. Figure 4(b) displays this amplitude (difference between resistances at $\theta = 90^\circ$ and $\theta = 0^\circ$) as a function of temperature. The maximum appearing at 15 K is due to the onset of scattering in the disordered region at the surface where most oxygen vacancies are generated. This scattering occurs when the radius of the classical orbit (and the mean free path) becomes comparable to the width of the confinement region, as proposed recently.[11]

Information about the width of the confinement zone can then be extracted from the magnetoresistance ratio for magnetic fields applied perpendicular and parallel to the plane (but always perpendicular to current). Notice that this ratio is roughly 3 at low temperatures. For magnetic fields perpendicular to the plane, orbital effects are limited by the electron mean free path ℓ. Using $\ell = \hbar k_F/R_s n_s e^2$ and $k_F = (3\pi^2 n_s/t)^{1/3}$, ℓ can be estimated as a function of the width of the confined layer. Notice that we have used the 3D expression for the relationship between carrier density and Fermi vector. Attempts to utilize the 2D expressions for $k_F = (2\pi n_s)^{1/2}$, using the sheet carrier density obtained from

the transport measurements, yields an unrealistically large value of the Fermi vector of 1.22×10^{11} m^{-1}, about one order of magnitude larger than the width of the first Brillouin zone for an STO crystal. The "thick" electron gas can still be regarded as 2D in the sense that the Fermi wavelength is shorter than the confinement width. This will be justified immediately below. The comparatively lower values of magnetoresistance for in-plane fields indicate that orbital motion is in this case limited by the size of the confinement zone, t. Since this magnetoresistance ratio (which by comparing Figs. 2 and 3 is estimated to be roughly 3 at low temperatures) scales as $(\ell/t)^2$,[23] it can be used to get an estimate of both ℓ and t. We have found a value of $\ell = 450$ nm for the electron mean free path at low temperature, an order of magnitude larger than the value of 25 nm estimated by Ben Shalom *et al.* for LAO/STO interfaces.[23] This suggests a width of the confinement zone of $t = 260$ nm, which can be used together with the sheet carrier density $n_s = 2.4\times10^{17}$ cm^{-2} obtained from Hall effect measurements at low temperatures to estimate bulk doping density levels in the range of $n_{3D} = 8.9\times10^{21}$ cm^{-3}. The values obtained for the width of the confinement zone are about one order of magnitude larger than those found for the 2D electron gas in LAO/STO interfaces.[24] Transport can be regarded as 2D because the mean free path is larger than the width of the confinement zone and the product $\ell k_F = 260\times10^{-9}\times6.9\times10^{9}$ (of the order of 1000) is greater that 1.

In the case of ion-beam-irradiated samples with 300 eV accelerating voltage,[15] carrier density profiles estimated from dynamic photoluminescence measurements[25] indicate widths of the metallic layer in the range of 60 nm. On the other hand, transport measurements of samples irradiated with similar energies and doses show micrometer-thick conducting layers, confirmed by positron annihilation experiments, suggesting that defect diffusion after irradiation may be an issue.[26] In our case, the different irradiation process (ion beam vs plasma etching in our case) does not allow a direct comparison of the energy ranges, although the 250 V dc bias obtained during irradiation may be considered a measure of the energy gain of Ar ions diffusing in the plasma. It may be thus regarded as a measure of the bombarding energy and it is not so different from the 300 eV set in ion-beam-irradiated samples. The conducting layer, hundreds of nanometers wide, is somewhat in between the extreme widths reported for ion-beam-irradiated samples.

The classical radius of the orbit can be tuned with the magnetic field to be larger than the width of the confinement region according to $R_c = \hbar k_F/eB$, a condition which, as described below, is fulfilled at low temperatures. Using $\ell = \hbar k_F/R_s n_s e^2$, the ratio ℓ/R_c between the electron mean free path and the radius of the classical orbit is $B/R_s n_s e$. This shows that, for a given magnetic field, since the sheet carrier density is almost constant in the whole temperature range, the ratio ℓ/R_c is essentially controlled by the temperature dependence of the sheet resistance. In other words, temperature can be used to tune the mean free path to be longer than the critical radius of the orbit, which will produce enhanced scattering if carriers reach the edges of the confinement region. An estimate of the classical radius yields $R_c = 420$ nm for an 8.5 T field, and the mean free path changes from $\ell = 128$ nm at 20 K to $\ell = 486$ nm at 5 K, showing that in fact ℓ/R_c becomes larger than 1 when the temperature is reduced. For the 260 nm estimated width of the confinement zone it is clear that below 20 K there will be a significant contribution from scattering at its edge, thus providing an explanation for the maximum observed in Fig. 4(b) for the MR amplitude.

An important issue is the homogeneity of the electron gas and the effect of possible inhomogeneities on the length scales (mean free path or width of the conducting sheet) obtained from the transport experiments. It has been shown that the magnetoresistance of high-mobility electron gases is largest for the Corbino geometry (circular-shaped sample with current contact at the center and periphery) and becomes smaller for bar-shaped samples which limit the orbital motion.[27] The squared samples used to measure transport in the van der Pauw geometry are thus adequate to probe the orbital motion although inhomogeneities in the electron gas may not be detected. However, bar-shaped samples are well suited to test the homogeneity of the electron gas.[27] In order to ascertain the inhomogeneity and effects of contact geometry, we cut the 5×5 mm^2 sample up with a diamond saw into three similar, 5×1 mm^2 bar-shaped pieces. The magnetoresistance of each piece was measured in a similar manner as presented above with the important difference that they had four in-line contacts. Figure 5 compares the van der Pauw geometry magnetoresistance of the original sample and the in-line results of the bar-shaped pieces. There are two van der Pauw curves corresponding to the two possible current directions (black and red lines) and three curves for the three new pieces (green, dark blue, and light blue lines). For the data presented in Fig. 5 the magnetic field was applied perpendicular to the surface of the samples at 50 K. This orientation and temperature were selected because the corresponding magnetoresistance is predominantly of orbital nature. There is rather limited deviation among the curves, indicating small lateral inhomogeneity of the magnetoresistance properties.

Next we describe the magnetoresistance under magnetic fields applied parallel to the current density. This configuration minimizes the Lorentz force and is relevant to examine

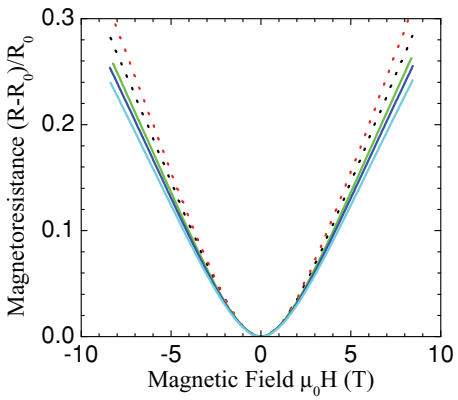

FIG. 5. (Color online) Magnetoresistance with field perpendicular to surface at $T = 50$ K for various geometries. Square 5×5 mm^2 sample with van der Pauw configuration in the two current geometries (black and red dotted lines), same sample cut into three individual pieces, with in-line 4-contact geometry (green, dark blue, light blue solid lines).

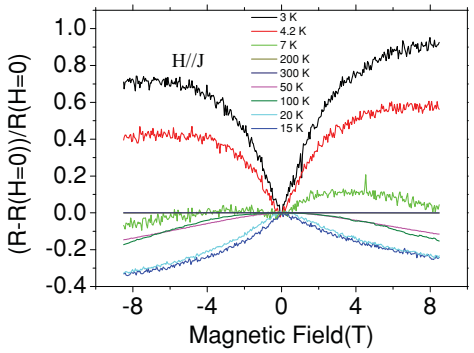

FIG. 6. (Color online) Magnetic field dependence of the magnetoresistance for magnetic fields applied parallel to the current direction. Different data sets correspond to different temperatures (3, 4.2, 7, 200, 300, 50, 100, 20, 15 K from top to bottom at 8 T) of a crystal irradiated at 30 W. Data have been normalized to the zero-field resistance.

transport phenomena free of the orbital effects which have been shown to be dominant due to confinement. Figure 6 shows the magnetic field dependence of the magnetoresistance at different temperatures. Data have been normalized to the zero-field resistance. Curves are essentially symmetric for positive and negative fields, although the slight asymmetry exhibited by some data sets is due to a small (spurious) Hall effect component, i.e., misalignment. While the expected vanishing magnetoresistance is found at high temperatures, below the structural transition of STO a large anomalous negative magnetoresistance develops. This magnetoresistance can be as high as 40% in 8 T fields at a temperature of 20 K. When the temperature is further lowered, the magnetoresistance abruptly changes sign and becomes positive. This behavior is reminiscent of the change in sign from negative to positive of the magnetoresistance previously found in 2D electron gases in the presence of spin-orbit interaction[28] and more recently also in LAO/STO interfaces.[29] But in these cases the magnetic field was applied perpendicular to the 2D layer, in contrast to our case. Negative magnetoresistance is typically ascribed to weak (anti)localization which is a (small) quantum correction to the conductivity.[30] However, it has an orbital origin and thus it is expected to show up only under transverse fields.[30] The longitudinal magnetoresistance of a 2D electron gas is expected to be dominated by electron-electron interaction effects and thus to be positive. Another explanation we can rule out is that the negative magnetoresistance originates in impurity band conduction. Many references exist in the literature pointing out the negative magnetoresistance of impurity band conduction, but typical values are at most a few percent.[31] We recall here that negative longitudinal magnetoresistances of comparable size were found in transport measurements in LAO/STO interfaces and attributed to the low-temperature antiferromagnetic state of the LAO/STO interface.[23] However, those samples did not show the positive low-temperature contribution to magnetoresistance, suggesting that the origin may be different. The large values found here suggest a magnetic origin as reported for semiconductors doped with paramagnetic transition metal ions.[31] The scattering of conduction electrons by localized moments is known to yield a negative magnetoresistance term scaling as the magnetization squared[32,33] due to the coupling of spin and momentum through the spin-orbit interaction. A spin-flip process results in momentum reversal due to the strong coupling between spins and momenta and consequently contributes to the resistivity. In our case the localized moments are Ti atoms in a +3 oxidation state as the result of oxygen vacancy doping. At low temperatures a fraction of these electrons may become localized at their impurity (vacancy) centers and acquire a paramagnetic moment, as reported in reduced samples.[34] The electric field gradients at impurities are known to couple electron momenta and spins.[35] In this scenario the relevant energy scale is the small 25 meV intra-atomic spin-orbit interaction of Ti^{3+}, and thus low temperatures are necessary to observe this effect. An additional source of (stronger) spin-orbit coupling may by the Rashba interaction due to electron confinement,[29,36] shown to have a strong effect on the more confined 2D electron gas at the LAO/STO interface. As recently suggested by Ben Shalom and co-workers,[36] spin-flip scattering may be important in limiting transport due to the spin-orbit coupling. Increasing the in-plane field will align moments and spin-flip scattering will not be important; thus the resistance is reduced and eventually saturated.

The crossover from negative to positive magnetoresistance when temperature is decreased occurs gradually, evidencing that magnetoresistance results from the addition of two terms, one negative and one positive, with a temperature-dependent ratio. This scenario has been observed in the past in semiconductors doped with transition metal impurities and discussed in terms of a two-band model that attributed the increase in magnetoresistance to a magnetic-field-controlled change of the relative occupation of two subbands with different mobilities.[24,37] This scenario applies well to STO,[38] where band structure calculations taking spin-orbit interaction into account have shown significant spin-orbit splitting of the Γ_{25} conduction band minimum at the center of the Brillouin zone below the cubic-tetragonal transition.[38] However, the positive magnetoresistance is only observed below 7 K far away from the structural transition, therefore putting in doubt that the transition itself is the origin of the positive MR. A different scenario for enhanced scattering at low temperatures can be found in the scattering of electrons at the edge of the confinement region when the radius of the orbit becomes comparable to its width. Although electrons driven in the direction of the current do not experience magnetic force, scattered electrons experience the magnetic force if the velocity with which they come out of a collision is not parallel to the magnetic field.[11] If the electron mean free path is longer than the classical radius of the orbit, orbital effects between collisions will allow scattered electrons to reach the disordered region at the edge of the confinement zone where most oxygen vacancies are concentrated, and enhanced scattering will occur. The estimate of the classical radius yields $R_c = 420$ nm and the mean free path changes from $\ell = 128$ nm at 20 K to $\ell = 486$ nm at 5 K, showing that in fact ℓ/R_c becomes larger than 1 when the temperature is reduced. This behavior is consistent with the change in sign of the magnetoresistance when temperature is lowered, as shown in Fig. 6. In the high-field limit the radius of the classical orbit becomes shorter than the width of the confinement region and the positive magnetoresistance effect disappears. On the other hand, at low fields the radius

of the classical orbit becomes so long that the condition $\ell/R_c > 1$ cannot be reached within the temperature window of the experiment. The progressive focusing of electron trajectories away from the surface when a magnetic field parallel to the current is increased (Chambers effect[39]) may also provide an explanation for the negative magnetoresistance observed. A final remark regards the possible temperature dependence of the width of the confinement region, which we have not taken into account. It is well known that the permittivity of STO displays a pronounced increase at low temperature, which might have an effect on the magnitude of the confining potential.[40,41] However, the strong electric field in the confinement region largely suppresses the permittivity increase at low temperatures.[11,24]

In summary, we have found evidence for confined transport in doped STO layers generated by Ar ion milling. Ar bombardment generates oxygen vacancies as confirmed by cathodoluminescence and x-ray photoemission spectroscopy. At the high doping levels of this work, we have estimated the width of the confinement zone in the 200 nm range, more than an order of magnitude larger than in the LAO/STO 2D electron gas at low temperatures. These results show that vacancies are created over much deeper length scales than the nanometer scale penetration of low-energy ions, suggesting that channeling may be playing a role. The large thickness of the confinement region allows orbital motion also for magnetic fields aligned in the plane directed perpendicular to the current direction. On analyzing transport with the magnetic field directed parallel to the current, we have found a negative magnetoresistance which we interpret as the signature of spin-orbit interaction in the transport experiment. A sign change in the magnetoresistance is found at low temperatures, which we interpret as the result of scattering in the disordered region at the surface where oxygen vacancies are created. These results support the view that the mobility increase at low temperature is controlled by the screening of the scattering potential of a disordered region where oxygen vacancies are generated. The large values of the sheet carrier density seem to suggest that these vacancies diffuse into deeper length scales. Our results are quite different from the findings of similar experiments on LAO/STO interfaces, indicating that the more confined electron gas in the LAO/STO case may be determinant, although we cannot discard the idea that a different origin of the metallic transport also plays a role in making transport properties different.

ACKNOWLEDGMENTS

This work was supported by Spanish MICINN Grant No. MAT 2008 06517, Consolider Ingenio Grant No. CSD2009-00013 (IMAGINE), and CAM Grant No. S2009-MAT 1756 (PHAMA).

[1] J. F Shooley, W. R. Hosler, and M. L. Cohen, Phys. Rev. Lett. **12**, 474 (1964).
[2] M. P. Warushawithana, C. Cen, C. R. Sleasman, J. C. Woicik, Y. Li, L. F. Kourkoutis, J. A. Klug, H. Li, P. Ryan, L. P. Wang, M. Bedzyk, D. A. Muller, L. Q. Chen, J. Levy, and D. G. Schlom, Science **324**, 367 (2009).
[3] A. Ohtomo and H. Y. Hwang, Nature (London) **427**, 423 (2004).
[4] N. Reyren, S. Thiel, A. D. Caviglia, L. F. Kourkoutis, G. Hammerl, C. Richter, C. W. Schneider, T. Kopp, A.-S. Ruetschi, D. Jaccard, M. Gabay, D. A. Muller, J.-M. Triscone, and J. Mannhart, Science **317**, 1196 (2007).
[5] A. D. Caviglia, S. Gariglio, N. Reyren, D. Jaccard, T. Schneider, M. Gabay, S. Thiel, G. Hammerl, J. Mannhart, and J.-M. Triscone, Nature (London) **456**, 624 (2008).
[6] G. Herranz, M. Basletic, M. Bibes, C. Carretero, E. Tafra, E. Jacquet, K. Bouzehouane, C. Deranlot, A. Hamzic, J. M. Broto, A. Barthelemy, and A. Fert, Phys. Rev. Lett. **98**, 216803 (2007).
[7] A. Kalabukhov, R. Gunnarsson, J. Borjesson, E. Olsson, T. Claeson, and D. Winkler, Phys. Rev. B **75**, 121404 (2007).
[8] P. R. Willmott, S. A. Pauli, R. Herger, C. M. Schleputz, D. Martoccia, B. D. Patterson, B. Delley, R. Clarke, D. Kumah, C. Cionca, and Y. Yacoby, Phys. Rev. Lett. **99**, 155502 (2007).
[9] D. W. Reagor and V. Y. Butko, Nature Mater. **4**, 593 (2005).
[10] V. Y. Butko, H. Wang, and D. Reagor, Nanotechnology **19**, 305401 (2008).
[11] J. H. Ngai, Y. Segal, D. Su, Y. Zhu, F. J. Walker, S. Ismail-Beigi, K. LeHur, and C. H. Ahn, Phys. Rev. B **81**, 241307 (2010).
[12] G. Koster, B. L. Kropman, G. J. H. M. Rijnders, D. H. A. Blank, and H. Rogalla, Appl. Phys. Lett. **73**, 2920 (1998).
[13] Y. Tokura, Y. Taguchi, Y. Okada, Y. Fujishima, T. Arima, K. Kumagai, and Y. Iye, Phys. Rev. Lett. **70**, 2126 (1993).
[14] M. Basletic, J. L. Maurice, C. Carretero, G. Herranz, O. Copie, M. Bibes, E. Jacquet, K. Bouzehouane, S. Fusil, and A. Barthelemy, Nature Mater. **7**, 621 (2008).
[15] D. Kan, T. Terashima, R. Kanda, A. Masuno, K. Tanaka, S. Chu, H. Kan, A. Ishizumi, Y. Kanemitsu, Y. Shimakawa, and M. Takano, Nature Mater. **4**, 816 (2005).
[16] D. Kan, R. Kanda, Y. Kanemitsu, Y. Shimakawa, and M. Takano, Appl. Phys. Lett. **88**, 191916 (2006).
[17] A. Rubano, D. Paparo, F. Miletto Granozio, U. Scotti di Uccio, and L. Marrucci, J. Appl. Phys. **106**, 103515 (2009).
[18] D. Drouin, A. R. Couture, D. Joly, X. Tastet, V. Aimez, and R. Gauvin, Scanning **29**, 92 (2007).
[19] O. L. Tufte and P. W. Chapman, Phys. Rev. **155**, 796 (1967).
[20] H. P. R. Frederikse, W. R. Thurbe, and W. R. Hosler, Phys. Rev. **134**, A442 (1964).
[21] O. L. Tufte and E. L. Stelzer, Phys. Rev. **173**, 775 (1964).
[22] S. Das Sarma and E. H. Hwang, Phys. Rev. Lett. **84**, 5596 (2000).
[23] M. Ben Shalom, C. W. Tai, Y. Lereah, M. Sachs, E. Levy, D. Rakhmilevitch, A. Palevski, and Y. Dagan, Phys. Rev. B **80**, 140403 (2009).
[24] O. Copie, V. Garcia, C. Bodefeld, C. Carretero, M. Bibes, G. Herranz, E. Jacquet, J. L. Maurice, B. Vinter, S. Fusil, K. Bouzehouane, H. Jaffres, and A. Barthelemy, Phys. Rev. Lett. **102**, 216804 (2009).
[25] H. Yasuda, Y. Yamada, T. Tayagaki, and Y. Kanemitsu, Phys. Rev. B **78**, 233202 (2008).

[26]G. Herranz, O. Copie, A. Gentils, E. Tafra, M. Basletic, F. Fortuna, K. Bouzehouane, S. Fusil, E. Jacquet, C. Carretero, M. Bibes, A. Hamzic, and A. Barthelemy, J. Appl. Phys. **107**, 103704 (2010).
[27]H. Weiss and H. Welter, Z. Phys. **138**, 322 (1957).
[28]G. Bergmann, Phys. Rev. Lett. **48**, 1046 (1982).
[29]A. D. Caviglia, M. Gabay, S. Gariglio, N. Reyren, C. Cancellieri, and J. M. Triscone, Phys. Rev. Lett. **104**, 126803 (2010).
[30]P. A. Lee and T. V. Ramakrishnan, Rev. Mod. Phys. **57**, 287 (1985).
[31]R. P. Khosla and J. R. Fischer, Phys. Rev. B **2**, 4084 (1970).
[32]K. Yosida, Phys. Rev. **107**, 396 (1957).
[33]M. Sawicki, T. Dietl, J. Kossut, J. Igalson, T. Wojtowicz, and W. Plesiewicz, Phys. Rev. Lett. **56**, 508 (1986).
[34]N. E. Phillips, J. C. Ho, D. P. Woody, J. K. Hulm, and C. K. Jones, Phys. Lett. A **29**, 356 (1969).
[35]R. J. Elliott, Phys. Rev. **96**, 266 (1954).
[36]M. Ben Shalom, M. Sachs, D. Rakhmilevitch, A. Palevski, and Y. Dagan, Phys. Rev. Lett. **104**, 126802 (2010).
[37]F. Reuss, S. Frank, C. Kirchner, R. Kling, Th. Gruber, and A. Waag, Appl. Phys. Lett. **87**, 112104 (2005).
[38]L. F. Matthiess, Phys. Rev. B **6**, 4740 (1972).
[39]R. G. Chambers, Proc. R. Soc. London, Ser. A **202**, 378 (1950).
[40]Z. Sefrioui, D. Arias, M. Verela, J. E. Villegas, M. A. Lopez de La Torre, C. Leon, G. D. Loos, and J. Santamaria, Phys. Rev. B **60**, 15423 (1999).
[41]X. J. Chen, H.-U. Habermeier, H. Zhang, G. Gu, M. Verela, J. Santamaria, and C. C. Almasan, Phys. Rev. B **72**, 104403 (2005).